EXPERIMENTAL VERIFICATION AND NUMERICAL EVALUATION OF THE THREE-INVARIANT DEPENDENT CAP MODEL FOR COHESIONLESS SOIL

S. N. Abul Abduljauwad*, M. O. Faruque, and M. Azeemuddin

Department of Civil Engineering
King Fahd University of Petroleum & Minerals
Dhahran, Saudi Arabia

الخلاصـــة :

لقد استخدم نموذج القلنسوة الذي يعتمد على الإجهادات الثلاثة غير المتغيرة لصياغة نموذج تكوين عام للتربة غير المتماسكة في إطار اللدانة التي لا تتغير مع الزمن وميكانيكا التربة ذات الحالة الحرجة. ولمعرفة مدى صلاحية هذا النموذج فقد اختبرت عينات من الرمل المحلي باستخدام جهاز ثلاثي المحاور معدّل. ولقد استخدمت نتائج هذه الاختبارات لحساب أحد عشر ثابتٍ للنموذج. ولوحظ قدرة النموذج على تنبؤ استجابة التربة للتجارب الثلاثية المحاور في حالة الإنضغاط والإطالة.

وتمّ ايضاح دقة النموذج واستخداماته المختلفة بإخضاعه لدراسة تصرف رمال الكثبان المحلية تحت تأثير قوى رتيبة مع السماح للماء بالنّزّ. وبعد ذلك تم استخدام النموذج في برنامج تجزئة محدودة لدراسة تفاعل قاعدة ضحلة مع التربة المساندة.

ABSTRACT

The concept of a three stress invariant dependent cap model is used to formulate a generalized constitutive model for cohesionless soils within the framework of rate independent plasticity and critical state soil mechanics. In order to assess the applicability of this model, a local sand is tested using a modified conventional triaxial device. The test results are used to evaluate the eleven model constants. The model is shown to realistically predict the soil response for triaxial experiments in both compression and extension.

The model's extreme versatility and accuracy are demonstrated by applying it to describe the behavior of the local dune sand under drained monotonic loading conditions. Thereafter, the use of the model in a finite element formulation for solving a boundary value problem is illustrated by using it to analyse the interaction of a shallow foundation with its supporting soil.

*Address for Correspondence:
KFUPM Box No. 608
King Fahd University of Petroleum & Minerals
Dhahran 31261, Saudi Arabia

EXPERIMENTAL VERIFICATION AND NUMERICAL EVALUATION OF THE THREE-INVARIANT DEPENDENT CAP MODEL FOR COHESIONLESS SOIL

INTRODUCTION

Stress-strain behavior of cohesionless soils is highly nonlinear and inelastic. Constitutive laws formulated within the framework of the theory of plasticity have been used in the past to characterize such nonlinear responses [1–7]. Of these models, the so called cap model proposed by DiMaggio and Sandler [1] is widely used for analyses of complex problems in geomechanics. The apparent popularity of this model stems from the fact that it is relatively simple to implement into existing numerical codes. Besides, the associated parameters of this model can be evaluated using conventional test data. Traditionally, conventional triaxial compression tests are performed in most soil mechanics laboratory. Often these test data are used to evaluate cap model parameters and eventually to verify the model itself. This would have been perfectly alright, if the soil responses were independent of the stress paths. In the case of cohesionless soils, stress-path dependency is quite significant. In particular, shear strengths of cohesionless soils along compression paths are different from those along extension paths. The original cap model, however, is not capable of describing this important aspect of cohesionless soils.

A modified cap model, proposed by Faruque [8], eliminates this deficiency and is thereby suitable for characterizing stress–strain responses of cohesionless soils.

The work presented in this paper includes testing of a local sand, parameter determination, and verification of the three-invariant dependent cap model, followed by the implementation of the model into a finite element scheme. In order to perform both extension and compression tests under constant mean pressure conditions, a conventional triaxial device is modified to become a stress-controlled device. This apparatus is then used to perform a series of triaxial extension and triaxial compression tests. Data obtained from the experimental program are used to evaluate an optimum set of parameters for the modified cap model. This set of parameters are used to predict stress–strain responses for a number of stress paths and the results are compared with experimental observations. As a final step, the model is implemented into a two-dimensional finite element code. A number of boundary value problems are solved using this computer procedure and the results are presented.

DESCRIPTION OF THE MODEL

The constitutive model utilized in this work is a modified cap model proposed by Faruque [8] which includes all three stress invariants in its formulation. This enables the model to characterize strength variations along compression and extension stress paths under constant mean pressure condition. In particular, J_1, J_{2D}, and θ are used for the mathematical description of the failure and yield surfaces which are expressed as

$$J_1 = \sigma_{kk} \tag{1}$$

$$J_{2D} = \tfrac{1}{2} S_{ij} \cdot S_{ij} \tag{2}$$

$$\theta = \tfrac{1}{3} \cos^{-1}\left[\frac{3\sqrt{3} J_{3D}}{2 J_{2D}^{3/2}}\right] \tag{3}$$

$$J_{3D} = \tfrac{1}{3} S_{ij} S_{jk} S_{ki} \tag{4}$$

where σ_{ij} is the stress tensor, $S_{ij} = \sigma_{ij} - \frac{\sigma_{kk}}{3} \delta_{ij}$ is the deviatoric stress tensor and δ_{ij} is the kronecker delta. The parameter θ denotes the orientation of the stress path on the octahedral plane which lies between 0° and 60°. In particular, $\theta = 0°$ corresponds to triaxial compression (TC) tests and $\theta = 60°$ corresponds to triaxial extension (TE) tests (Figure 1).

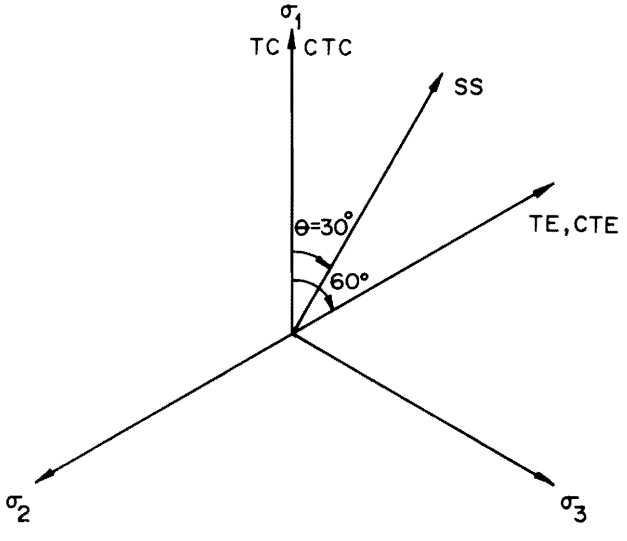

Figure 1. Stress Paths on the Octahedral Plane.

Equation of the Failure Surface

The equation of the fixed failure surface as proposed in the model can be written as

$$F_f = g(\theta,J_1)\sqrt{J_{2D}} - A - MJ_1 - C\exp(-BJ_1) = 0 \quad (5)$$

where A, B, C, and M are material constants associated with the failure states of a material point and $g(\theta,J_1)$ is a shape function expressed in the form

$$g(\theta,J_1) = \frac{2}{\sqrt{3}}\cos[\tfrac{1}{3}\cos^{-1}(-A_t \cdot \cos 3\theta)] \quad (6)$$

where

$$A_t = A_o \cdot \exp(-\gamma \cdot J_1/p_a) \quad (7)$$

The parameter A_o in Equation (7) is a constant and should be chosen in such a manner so as to satisfy the convexity of the failure surface on the octahedral plane. This defines the range of the permissible values of A_o. Specific value of A_o is then chosen based on the observed limiting shapes of the failure surface on the octahedral plane. Analysis of the shape function, $g(\theta,J_1)$, reveals that the range $0 \leq A_o \leq 1$ satisfy convexity requirements of the failure surface on the octahedral plane [9]. The extreme values of A_o in the general range signify possible limiting shapes of the failure surface. In particular $A_o = 0$ eliminates the dependency of the failure surface on the parameter, θ and thereby is suitable for materials whose shear strength is independent of θ. On the other hand, $A_o = 1$, defines a triangular failure surface with rounded corners in the absence of J_1. This behavior is reasonable for materials like concrete, rocks as well as cohesionless soils. In view of this, $A_o = 1$ is used in the present work. In Equation (7), p_a is the atmospheric pressure expressed in the same units as J_1 and γ is a material constant which describes the change in the shape of the failure surface on the octahedral plane as J_1 increases. Typical cross-sections of the failure surface for different values of J_1 are depicted in Figure 2. It is evident that as J_1 becomes very high (theoretically $J_1 \rightarrow \infty$), the failure cross-section becomes almost circular (see Figure 2). On the other hand, for a relatively low value of J_1, the cross-section is triangular with rounded corners (Figure 2). This behavior is in agreement with the experimental observations for a number of engineering materials including cohesionless soils. Typical plots of Equation (5) on $\sqrt{J_{2D}} - J_1$ space for different values of θ are shown in Figure 3.

Equation of the Yielding Cap

The following form of yield cap is defined in the model:

$$F_c = g(\theta,L)\sqrt{J_{2D}} - \sqrt{b^2 - (J_1 - L)^2/R^2} = 0 \quad (8)$$

where $g(\theta,L) = g(\theta,J_1 = L)$, L is the value of J_1 at the point of the intersection of the yield cap and the failure surface (see Figure 3) and b is expressed as

$$b = A + ML - C\exp(-BL) \quad (9)$$

The parameter R in Equation (8) is a material constant which denotes the shape of the elliptical yield cap. Geometrically, it is the ratio of the horizontal axis to the vertical axis of the elliptical cap.

The soils generally experience strain hardening during inelastic deformation. In the cap model, this behavior is described by allowing the expansion of the yield cap. As reported by DiMaggio and Sandler [1], the expansion of the cap can be modelled by expressing X (see Figure 3) in terms of accumulated plastic volumetric strain, ε_v^p i.e.

$$X = -\frac{1}{D}\ln\left(1 - \frac{\varepsilon_v^p}{W}\right) + Z \quad (10)$$

where D, W, and Z are the material constants which describe strain hardening. The physical meaning of these parameters can be found elsewhere [1, 10, 11].

SAND USED AND THE TESTING PROGRAM

The sand used in the investigation was obtained from the King Fahd University beach in Dhahran, Saudi Arabia. The sand was dry and the grain size distribution analysis indicated that the soil is uniformly graded with about 80% of grains between the sized of 0.149 mm and 0.420 mm. The physical properties and shear strength parameters are shown in Table 1.

The present model formulation is best fitted to describe the response of cohesionless soils. This form of cap model employs a total of eleven material parameters. Essentially there are 3 sets of model parameters:

(1) Elastic parameters (E,ν);

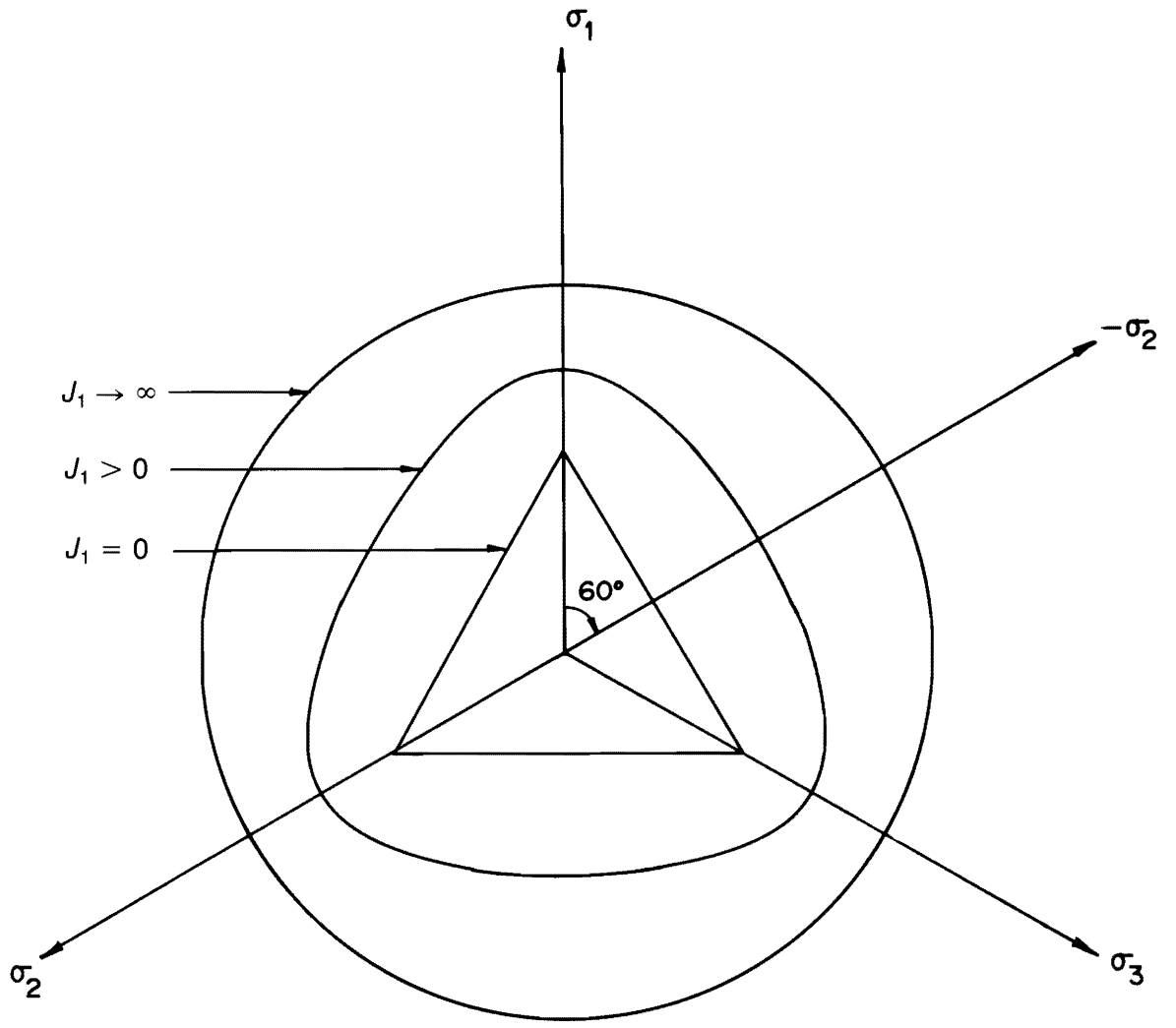

Figure 2. Failure Surface on the Octahedral Plane for Limiting Values of J_1.

(2) Failure surface parameters (A, B, M, C, γ);

(3) Hardening surface parameter (D, W, R, Z).

The determination of these parameters for Dhahran dune sand will require a set of conventional triaxial compression tests under wide range of confining pressures with cycles of unloading and reloading, triaxial compression and triaxial extension tests carried to failure and hydrostatic test with cycles of unloading and reloading.

The available testing device at King Fahd University consisted of a vertical strain controlled conventional triaxial testing apparatus for cylindrical samples. The usage of this device will be limited to conventional triaxial compression tests only. This classical device was modified for conducting stress controlled tests where the axial stress and the lateral stress are controlled independently. The modified apparatus depicted in Figure 4 consists of σ_1 chamber which is completely isolated from the triaxial cell. This allows one to test samples under a wide variety of stress paths by independently varying the axial stress, σ_1, and the lateral stress, σ_3. The extra weight of the piston in σ_1 chamber is nullified by using a load balancing system.

For laboratory investigations, cylindrical samples of 2.8 in diameter were prepared of the dry sand with a length to diameter ratio of 2. A constant density of 1.68 g/cm^{-3} was achieved consistently by controlling the height of drop for sand and rotating the pouring funnel in a circular manner during the fall of the soil. Saturation was achieved by replacing air inside the

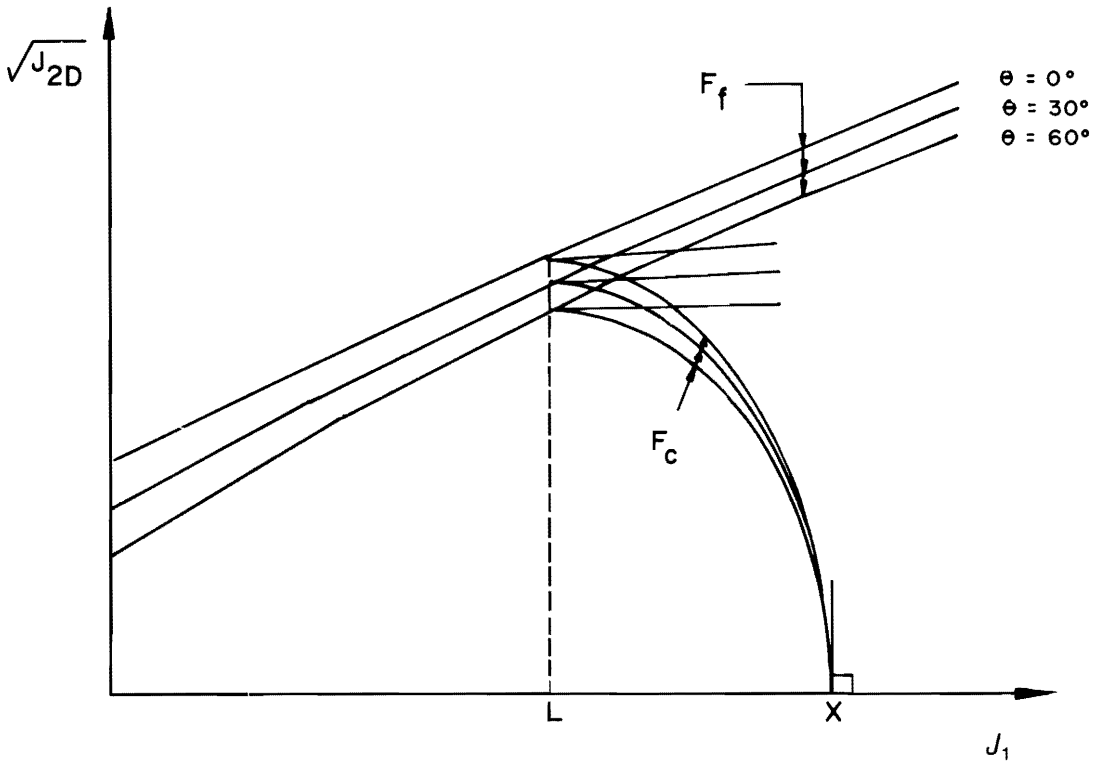

Figure 3. Failure and Yield Surfaces for the Three Invariant Dependent Cap Model.

Table 1. Summary of Test Results for Sand.

Max. density (kN/m^3)	17.71
Min. density (kN/m^3)	14.73
Measured density (kN/m^3)	16.40
Relative density (%)	83.4
D_{10}(mm)	0.15
Uniformity coefficient $C_u = \frac{D_{60}}{D_{10}}$	1.84
Coefficient of curvature $C_c = \frac{D_{30}^2}{D_{10} * D_{60}}$	0.998
Angle of friction (φ)	33.0°
Cohesion (C) kN/mm^2	0.0

samples by carbon dioxide, CO_2, and applying a back pressure. The axial displacement of samples were measured by a linear variable displacement transducer. The radial strains were calculated from the volumetric strains which were measured by the amount of water draining out or into the sample.

THE TEST RESULT

The conventional triaxial compression tests were conducted at a confining pressure varying from 5 psi to 40 psi at 5 psi interval, and at 50 psi, 60 psi, and 100 psi. The deviator stress *versus* axial and radial strain for a sample under all around pressure of 30 psi (207 kPa) with two cycles of unloading and reloading is shown in Figure 5. It can be observed that the radial strain is about 60% of the axial strain. The corresponding volumetric strain shown in Figure 6 indicated the existence of small initial compression followed by a large amount of dilation.

The truly triaxial tests were performed at a confining pressure of 20 (138 kPa) and 30 psi (207 kPa) on the modified stress controlled device. In these tests, the stress is applied in such a way that the mean

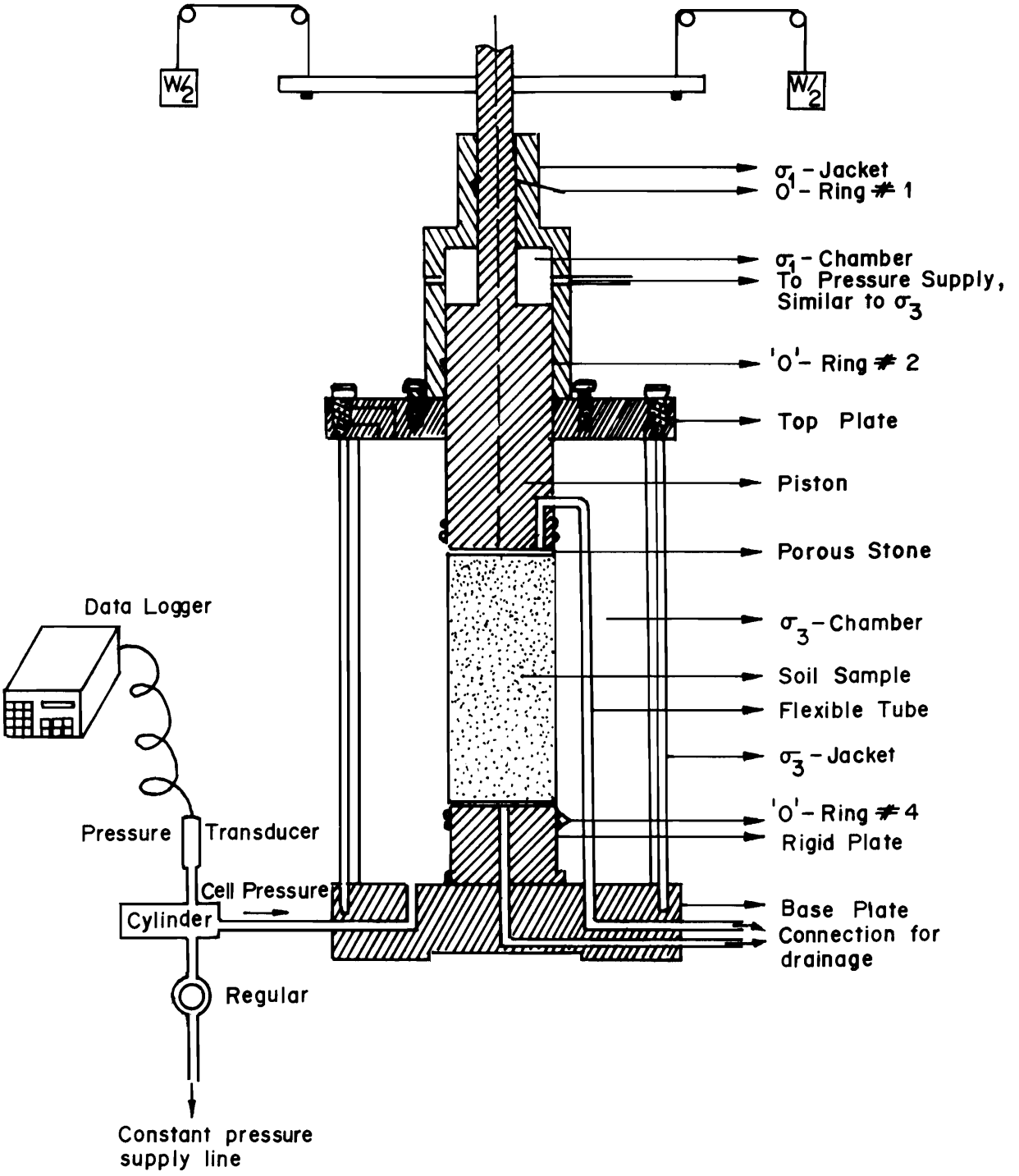

Figure 4. Diagrammatic Sketch of the Modified Triaxial Apparatus.

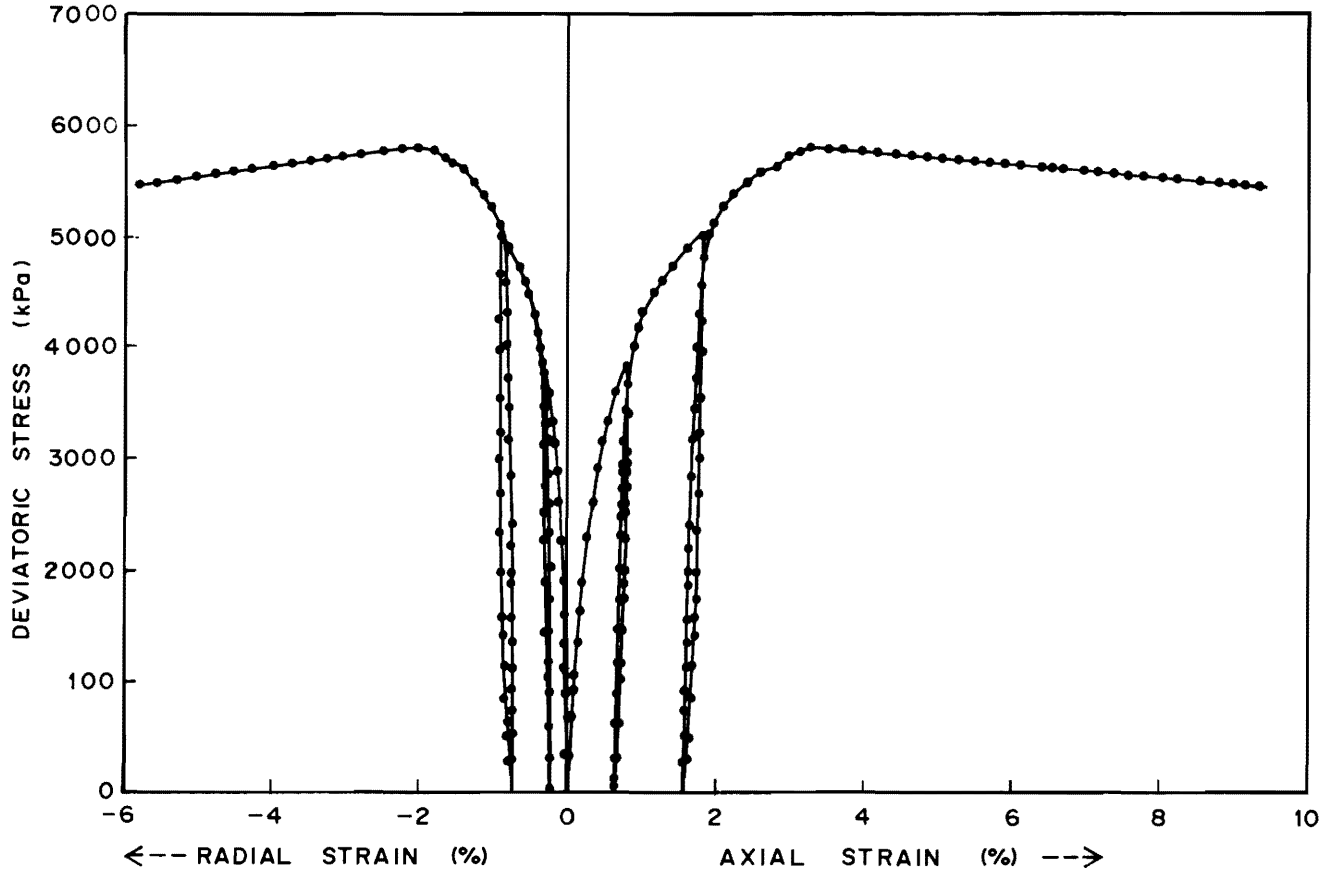

Figure 5. Experimental Stress–Strain Curve for CTC Test at 207 kPa (30 psi).

Figure 6. Volume Change for CTC Test at 207 kPa (30 psi).

pressure remain constant throughout the test. In case of a truly triaxial compression test (TC) σ_1 is increased while σ_2 and σ_3 ($\sigma_2 = \sigma_3$) are reduced by half the amount so that the net change in the mean pressure, $(\Delta\sigma_1 + \Delta\sigma_2 + \Delta\sigma_3) = 0$. Figure 7 shows the result of TC test for a sample under a confining pressure of 30 psi (207 kPa). For the truly triaxial extension test (TE), σ_1 is reduced while σ_2 and σ_3 are increased by half the amount. Figure 8 shows the deviator stress vs strain curves for 30 psi (207 kPa) confining pressure. It can be seen from the above figures that for the same confining pressure, the samples show lower strength in the extension test than that in the compression test.

The result of the hydrostatic compression test (HC) is depicted in Figure 9 where the mean pressure is plotted as a function of the volumetric strain. It is noted that K (bulk modulus, slope of p *versus* ε_v curve) increases with the mean pressure. Also note that the unloading reloading portion of the response is nonlinear. This shows that the elastic bulk modulus of cohesionless soil is a function of the confining pressure.

DETERMINATION OF MODEL PARAMETERS AND BACKPREDICTIONS

The constitutive model utilized in this work has eleven (11) material constants including the elastic constants E (Young's modulus) and ν (Poisson's ratio). The elastic constants E and ν can be directly determined using the unloading-reloading responses obtained from CTC, TC, and TE tests. The detailed procedure for the determination of E and ν is reported by Faruque [12].

Besides the elastic constants, there are nine (9) additional constants (A, B, C, M, γ, R, D, W, Z) which are related to the inelastic response of soils. Of these, γ is the only additional parameter introduced in the modified cap model. The constants A, B, C, M, R, D, W, and Z (which are essentially the same parameters in the two-invariant cap model) can be evaluated from the laboratory test data using standard procedures [4, 10]. This, however, requires the evaluation of the parameter γ prior to the evaluation of A, B, C, M, R, D, W, and Z. A procedure suggested by Faruque [8] can be conveniently used

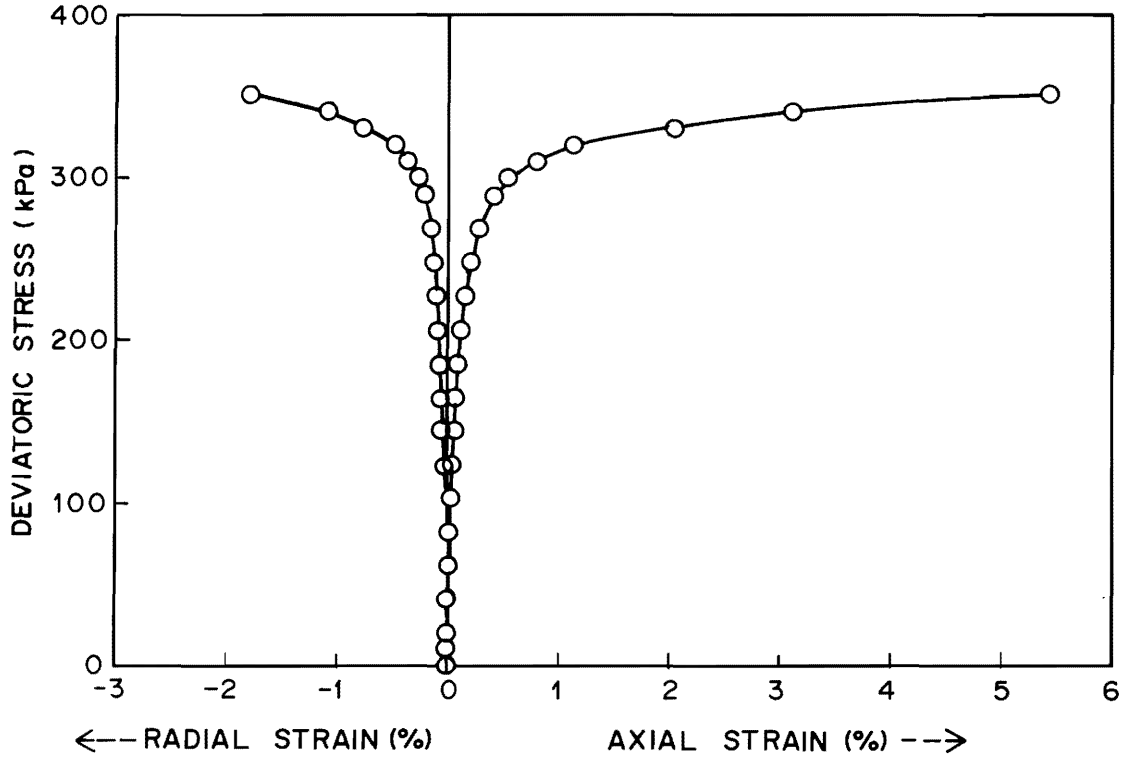

Figure 7. Experimental Stress–Strain Curve for TC Test at 207 kPa (30 psi).

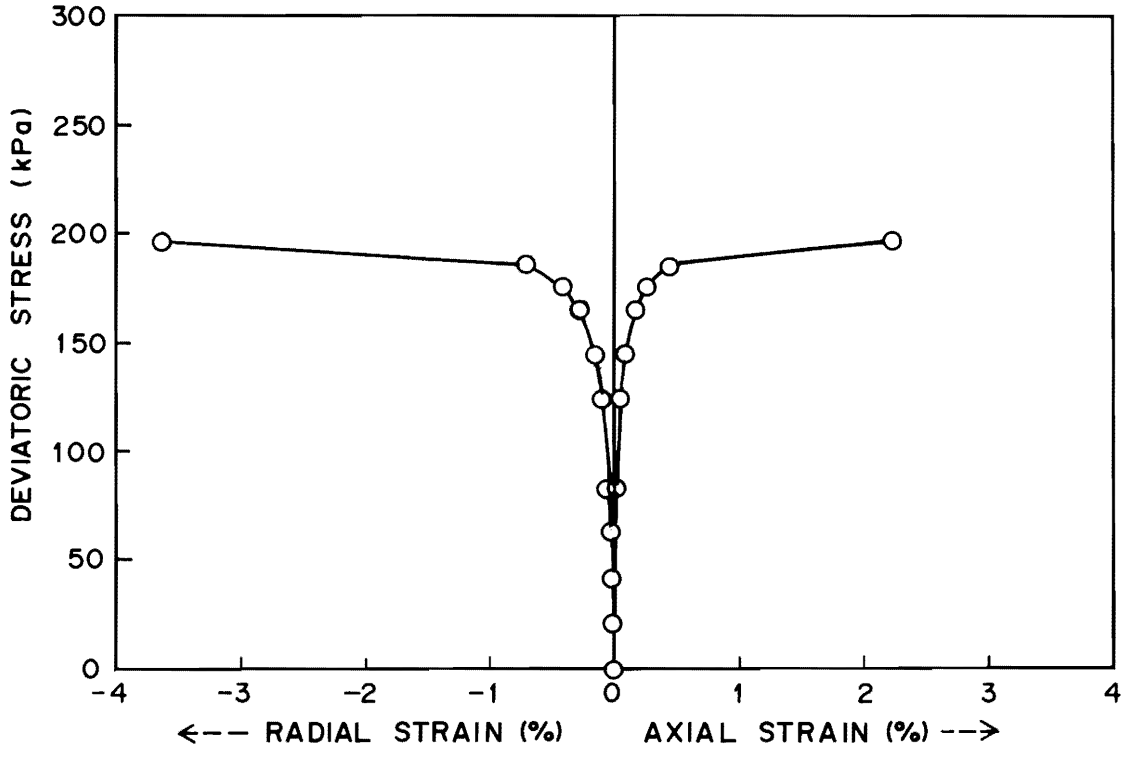

Figure 8. Experimental Stress–Strain Curve for TE Test at 207 kPa (30 psi).

Figure 9. Experimental Hydrostatic Compression Curve.

to evaluate the parameter, γ, which utilizes test data for a TC and a TE test both performed at the same mean confining pressure (or J_1).

The equation of the failure surface (Equation 5) can be specialized for the TC and TE tests as:

$$g_0\sqrt{J_{2D}^0} = A + MJ_1 - C\exp(-BJ_1) \quad (11)$$

$$g_{60}\sqrt{J_{2D}^{60}} = A + MJ_1 - C\exp(-BJ_1) \quad (12)$$

where $\sqrt{J_{2D}^0}$ and $\sqrt{J_{2D}^{60}}$ are the values of $\sqrt{J_{2D}}$ at failure for the TC and the TE test, respectively and g_0 and g_{60} are the values of $g(\theta,J_1)$ for $\theta = 0°$ and 60°, respectively. Since J_1 is the same for both tests, right hand sides of Equations (11) and (12) are the same. This allows one to write:

$$g_0\sqrt{J_{2D}^0} = g_{60}\sqrt{J_{2D}^{60}}. \quad (13)$$

Since J_1, $\sqrt{J_{2D}^0}$ and $\sqrt{J_{2D}^{60}}$ are known, Equation (13) can be solved numerically to obtain the parameter, γ.

The experimental results reported in the previous section are used to evaluate all eleven material constants mentioned previously. Determination of these constants are discussed in detail by Faruque and Abduljauwad [13]. The following set of parameters are obtained for the local dune sand:

$E = 25780 + 756\,p$ (kpa)	$M = 0.18$
$\nu = 0.34$	$R = 7.0$
$A = 17.24$ kPa	$D = 8.7 \times 10^{-4}$/kPa
$B = 5.86 \times 10^{-4}$/kPa	$W = 0.0085$
$C = 17.24$ kPa	$Z = 0.0$
$\gamma = 0.008$	

The above set of material constants are then used to backpredict the responses of a number commonly performed laboratory tests. In order to facilitate backpredictions of various tests utilizing the proposed model, a FORTRAN computer program has been developed where the input variables are the incremental stresses. The computer program determines the corresponding incremental strains using the so called subincrementation technique [12].

The first test considered in the backprediction is the hydrostatic compression test. Figure 10 shows the model predictions along with the experimental data. Evidently, a good agreement is achieved.

For shear tests, three sets of backpredictions along with experimental observations are considered in this paper.

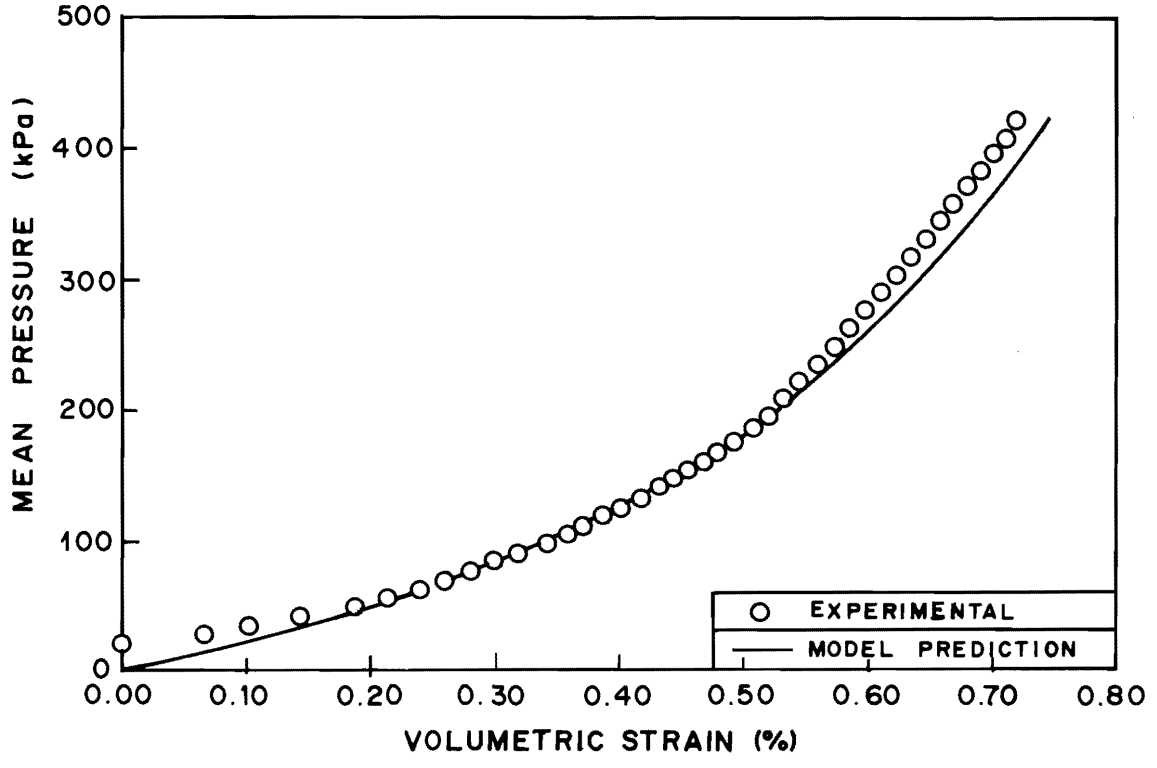

Figure 10. Backprediction of Hydrostatic Compression Test.

The back predictions of two CTC (conventional triaxial compression) tests constitute the first set and the results are shown in Figure 11, (*a*) and (*b*). Figure 11(*a*) shows the comparison between prediction and experimental observation for a CTC test at a confining pressure of 25 psi (172.5 kPa). Figure 11(*b*) shows a similar comparison for a CTC test at a confining pressure of 40 psi (276 kPa). Evidently, model predictions compare quite well with the experimental results.

Figure 12(*a*) and (*b*) show the comparison between model predictions and experimental data, for two TC (triaxial compression) tests at mean pressures of 20 psi (138 kPa) and 30 psi (207 kPa), respectively. Similar comparisons for two TE (triaxial extension) tests are shown in Figure 13(*a*) and (*b*) at constant mean pressures of 20 psi (138 kPa) and 30 psi (207 kPa), respectively.

It is evident from figures 12 and 13 that the model predictions are in agreement with the experimental observations. In particular, the model is quite effective in characterizing strength variations along compression and extension paths.

APPLICATION TO THE ANALYSIS OF SHALLOW FOUNDATION

The model was coded and incorporated in a finite element code called MICROFEM. The numerical work was based on an incremental iterative procedure using the tangential stiffness method.

In the finite element analysis, a load increment is applied and trial solutions for stress and strain at the Gaussian integration points are obtained. Since the material response is elasto-plastic, these solutions for stress and strain do not satisfy the elasto-plastic constitutive relations. Therefore, a procedure is required to estimate the correct stress corresponding to the calculated strains at the Gaussian integration points. In this work, the subincremental method is used to estimate stresses consistent with the elasto-plastic constitutive model [15]. The first step in the subincrementation procedure is to divide $\Delta\varepsilon_{ij}$ into a number of subincremental strain $\Delta\varepsilon^{s}_{ij}$, such that the absolute value of the components in $\Delta\varepsilon^{s}_{ij}$ is less than a prescribed small number [14]. The second step is to compute the subincremental stress $\Delta\sigma^{s}_{ij}$, using the elasto-plastic constitutive matrix at the end of the previous subincrement. The incremental stress is computed by summing the subincremental stresses. Mathematically this can be written as:

$$\Delta\sigma_{ij} = \sum_{k=1}^{N} (C^{ep}_{ijkl})_{k-1} \cdot \Delta\varepsilon^{s}_{kl} \qquad (14)$$

where $(C^{ep}_{ijkl})_{k-1}$ is the elasto-plastic constitutive tensor computed at the end of $(k-1)$th subincrement.

A simple, well known, problem of a strip foundation was considered to evaluate the ability of the model to simulate the interaction between the cohesionless soil mass and the foundation. The soil mass below the footing was modelled by means of finite element using a four noded quadrilateral element. The geometry and boundary conditions of the problem are shown in Figure 14. The behavior of flexible as well as rigid footing are investigated. The in-situ stresses are assumed to constitute the initial state prior to the application of external loading to the footing.

The computed load-settlement response curves at the center and edge of the foundation for both flexible and rigid footings are shown in Figure 15 and Figure 16 respectively. Also, a comparison with elastic solutions are presented in these figures.

Comparison between the average load–settlement curves of flexible and rigid foundation is made in Figure 17, where the average stress is plotted against the average displacement. Figures 18 & 19 represent the displacement field, where the short line segments indicate the direction and the size of total displacement values for each node at 158 kPa load level. In these figures the displacement vectors are drawn on an exaggerated scale. In the case of flexible footing, the soil beneath the footing moves downwards non-uniformly while uniform displacement can be observed under the rigid footing. Moreover, the displacement vectors indicated flow outwards and down from the footing. This is followed by a transition zone where the displacement vectors start to change direction. Finally, the vectors are directed outwards and upward. Figures 20 & 21 show the corresponding deformed mesh.

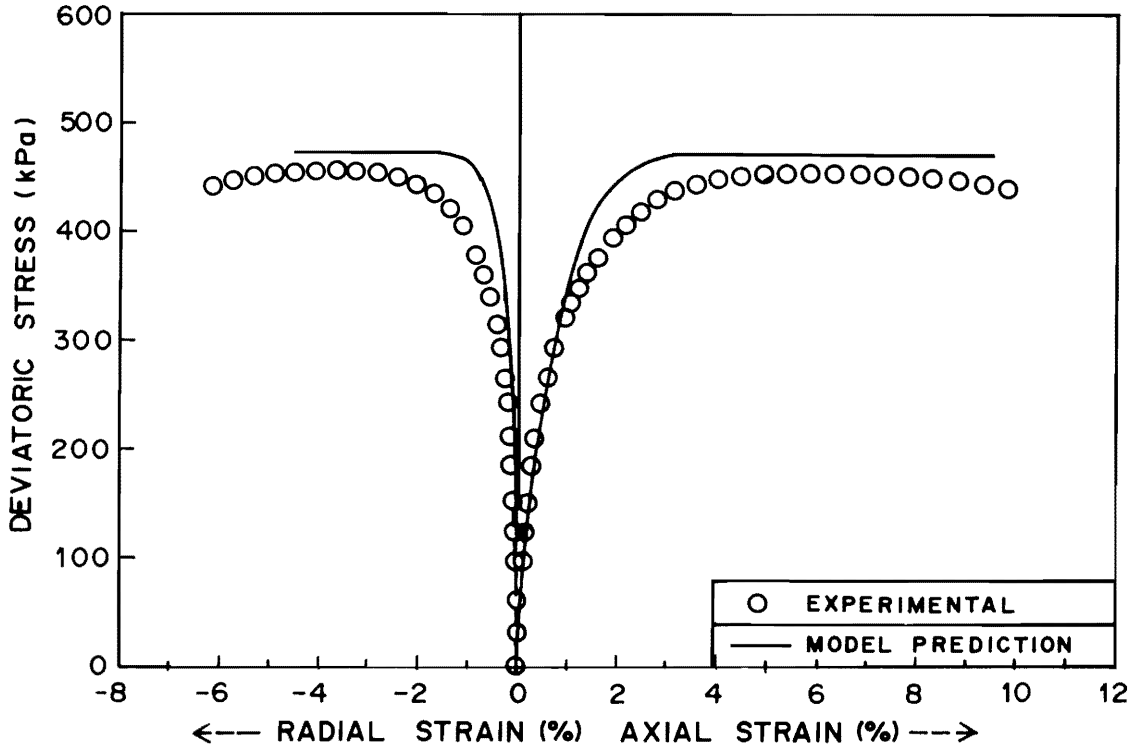

Figure 11a. Comparison of Stress–Strain Response for CTC Test at 172.5 kPa (25 psi).

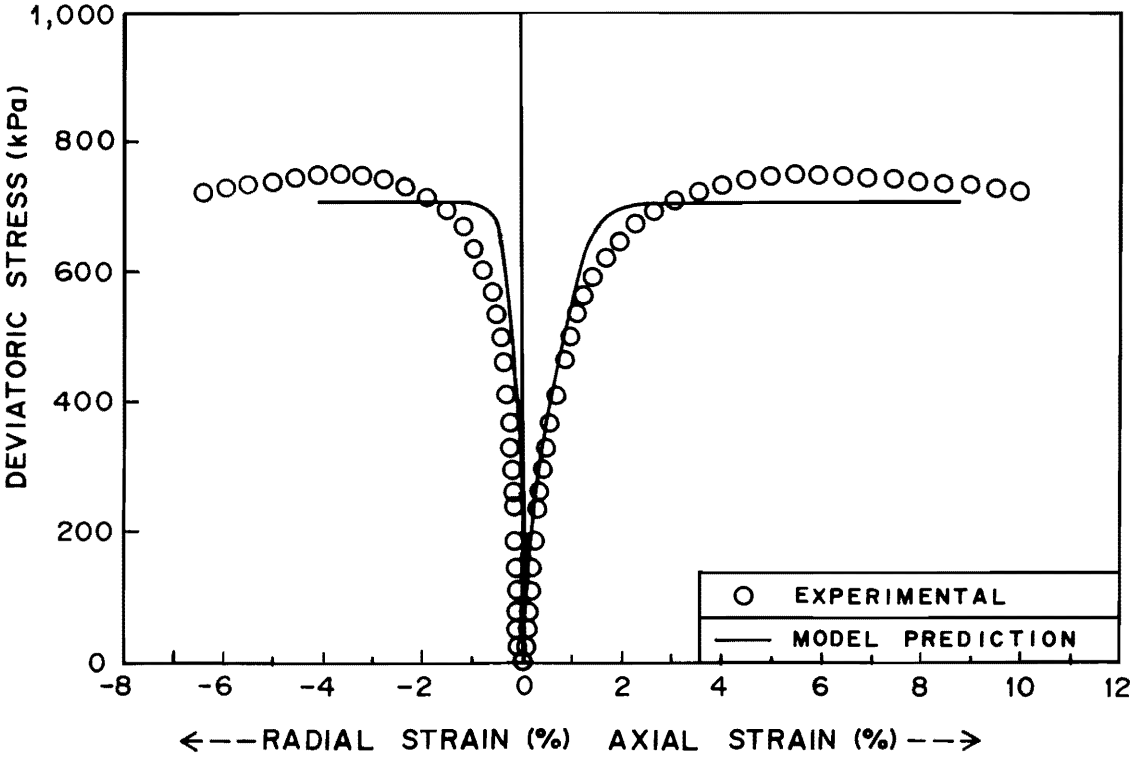

Figure 11b. Comparison of Stress–Strain Response for CTC Test at 276 kPa (40 psi).

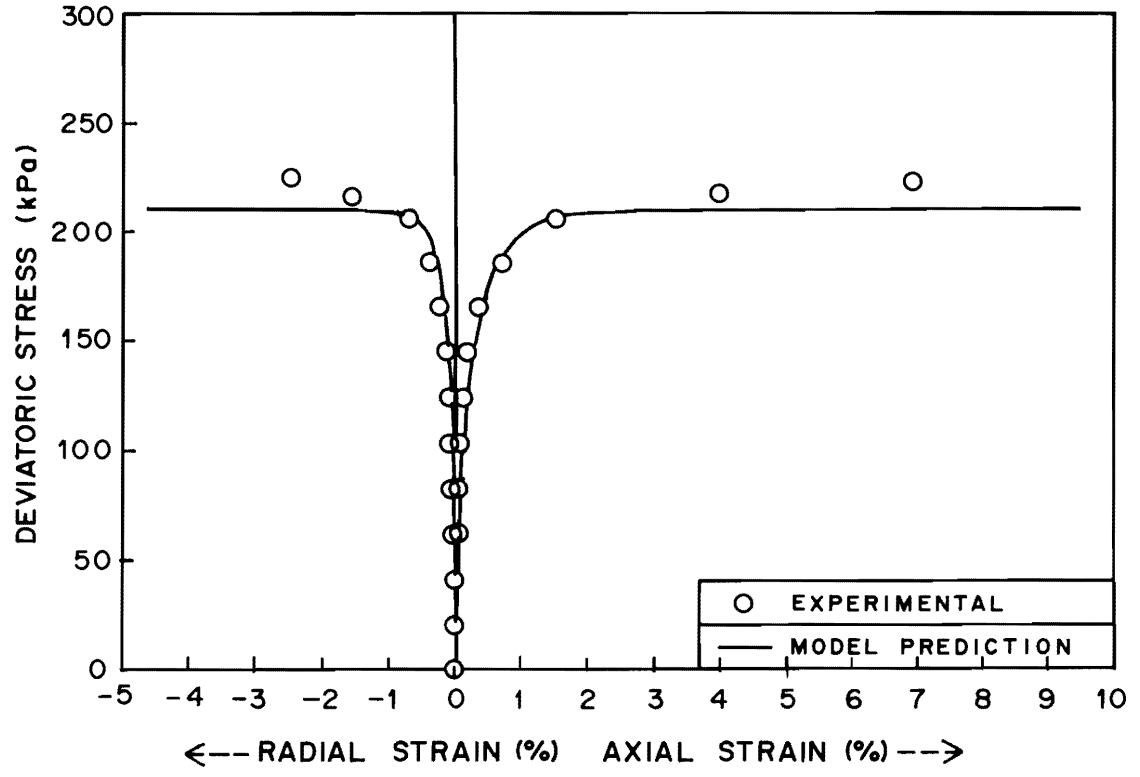

Figure 12a. Comparison of Stress–Strain Response for TC Test at 138 kPa (20 psi).

Figure 12b. Comparison of Stress–Strain Response for TC Test at 207 kPa (30 psi).

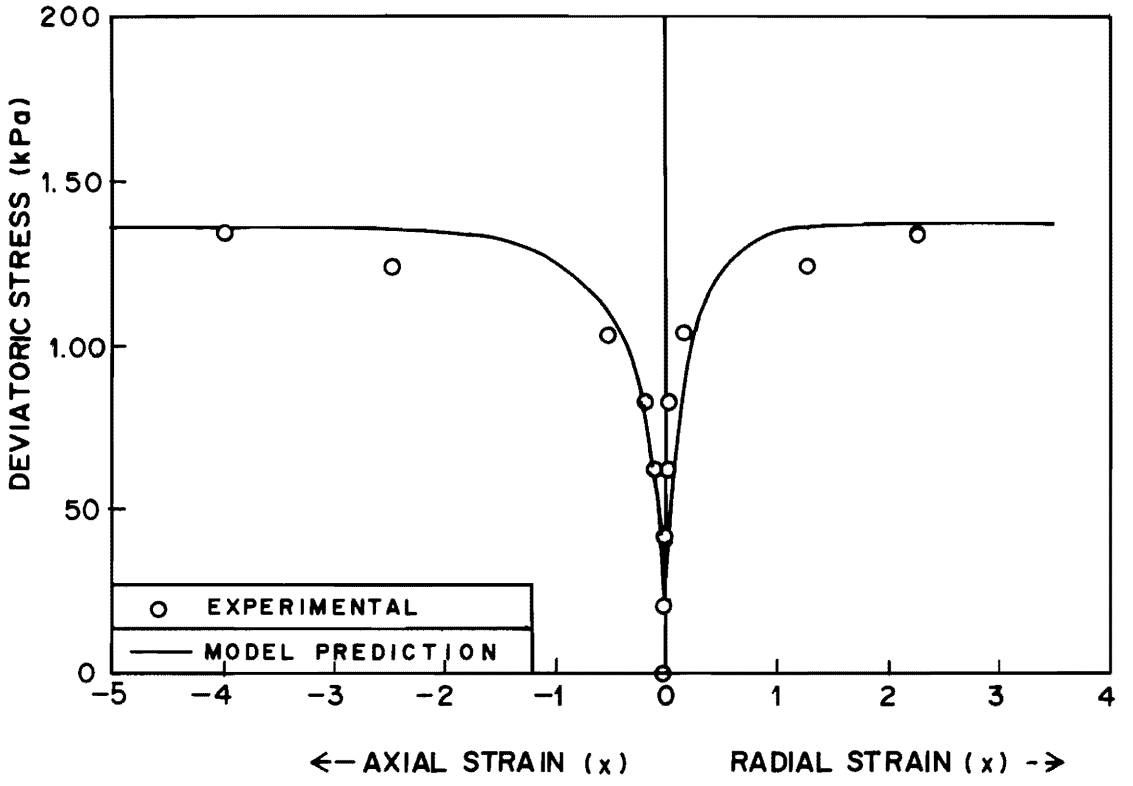

Figure 13a. Comparison of Stress–Strain Response for TE Test at 138 kPa (20 psi).

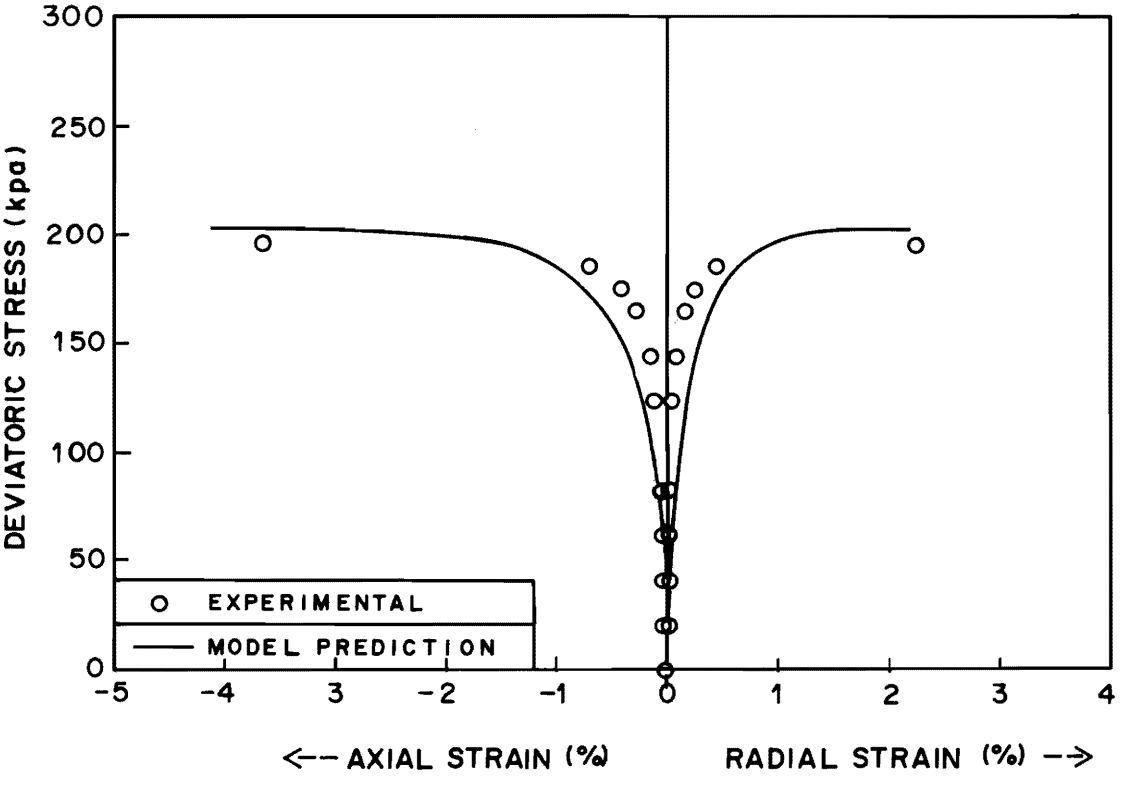

Figure 13b. Comparison of Stress–Strain Response for TE Test at 207 kPa (30 psi).

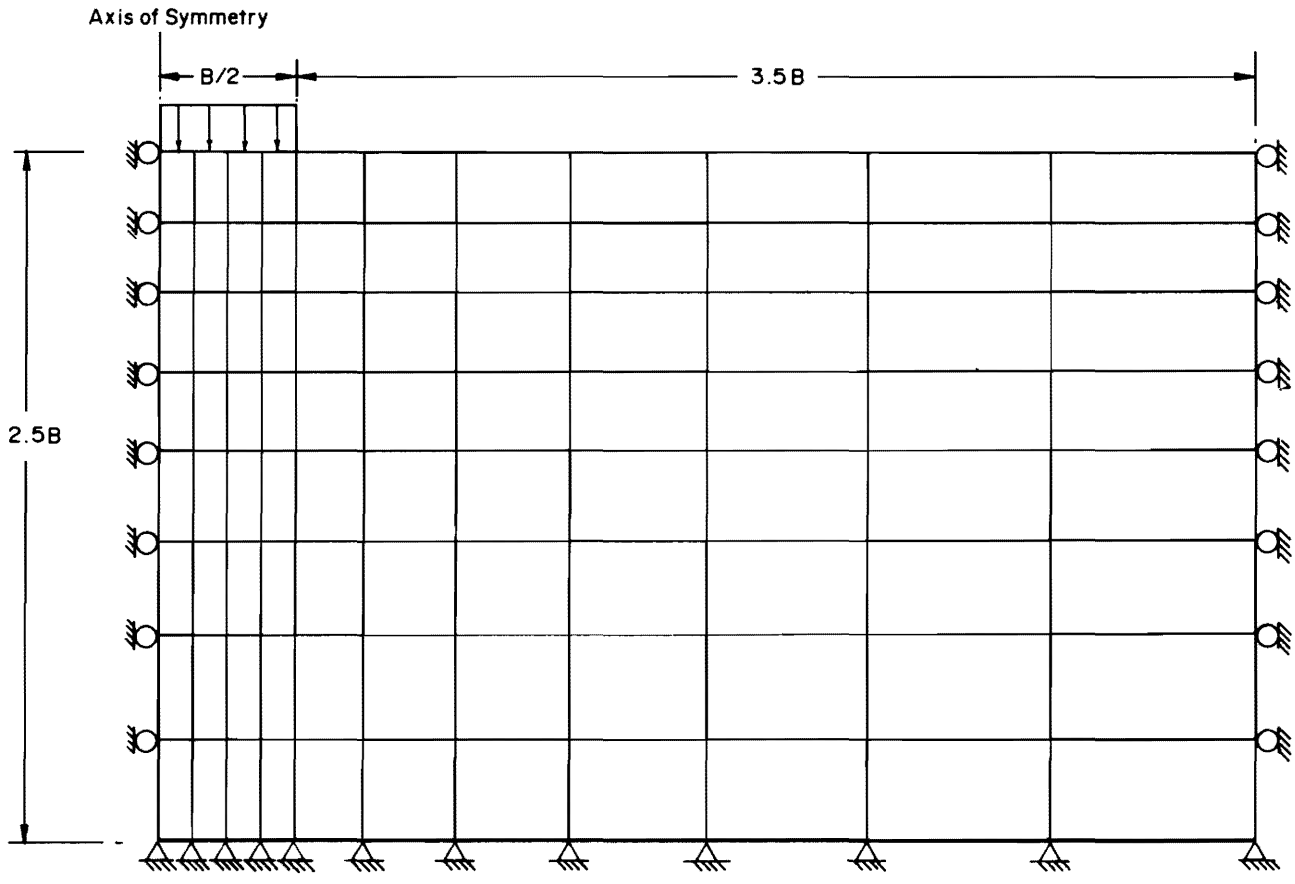

Figure 14. Finite Element Mesh for the Strip Footing.

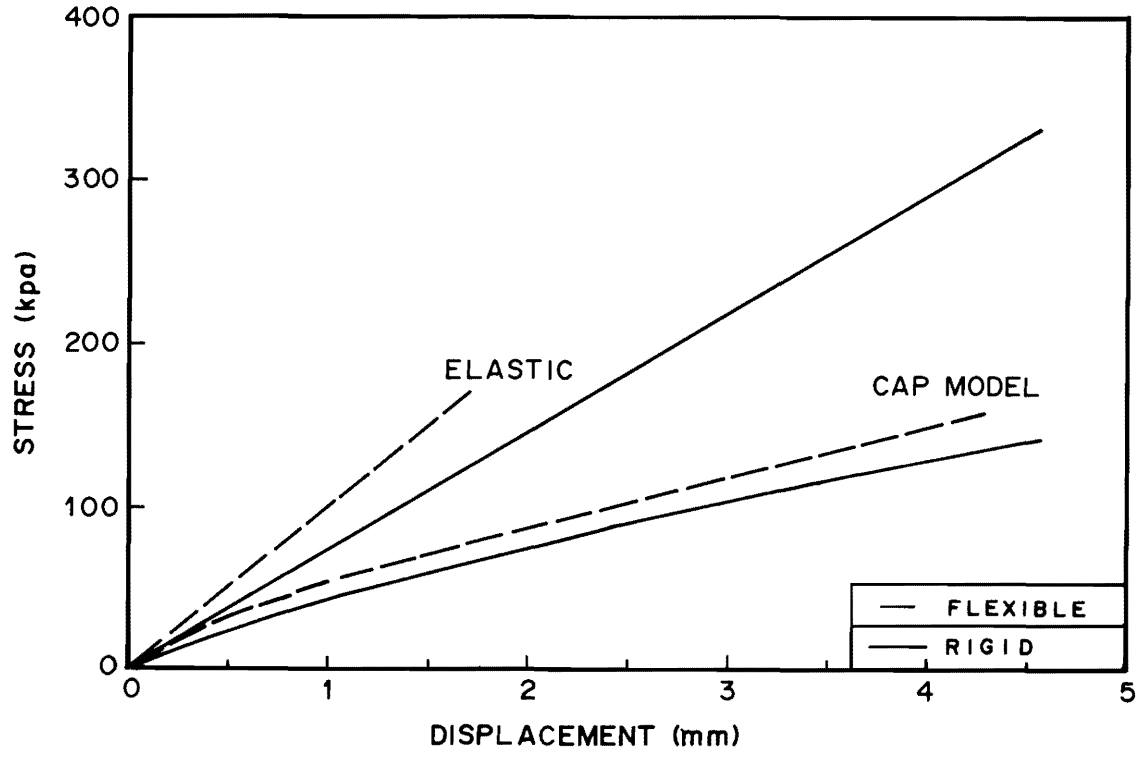

Figure 15. Load–Settlement Curve at the Center of the Foundation.

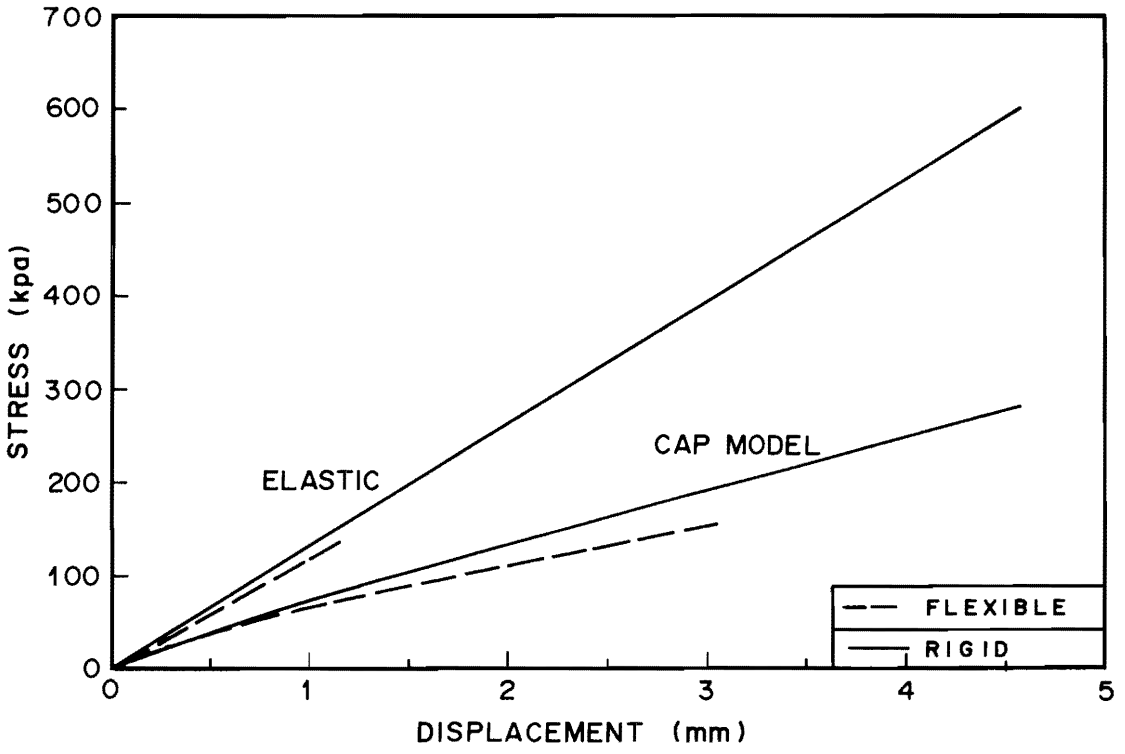

Figure 16. Load–Settlement Curve at the Edge of the Foundation.

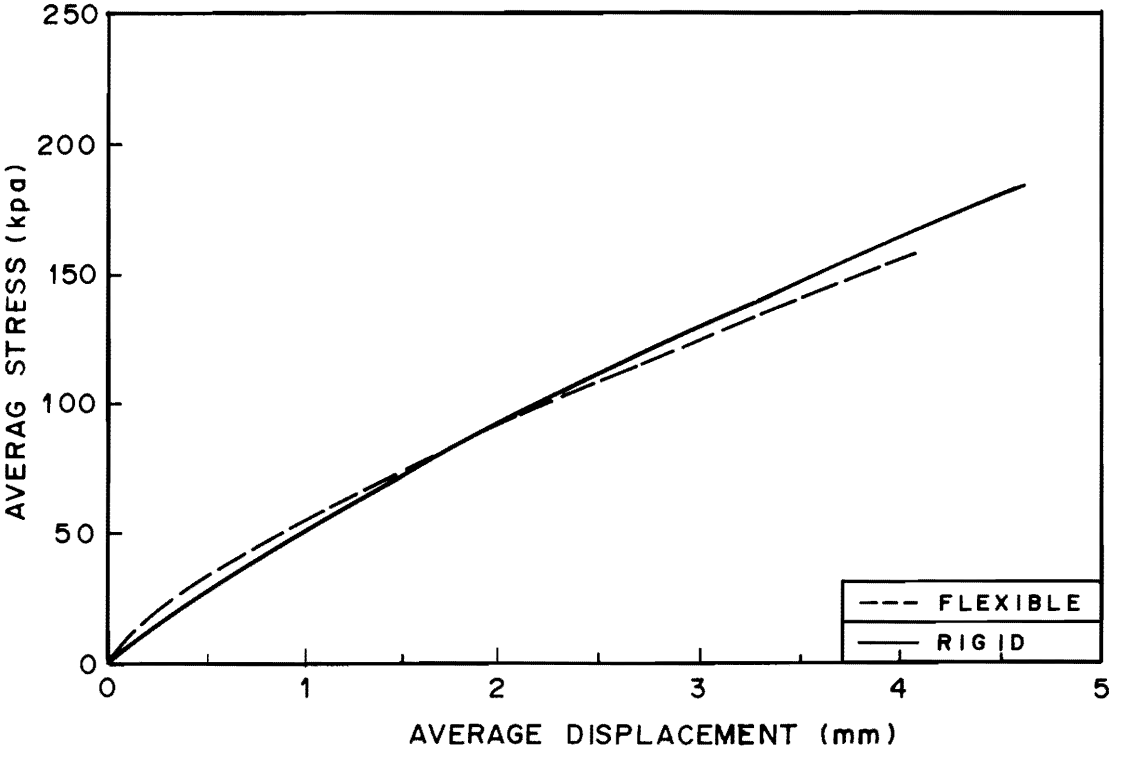

Figure 17. Average Load–Settlement Curve.

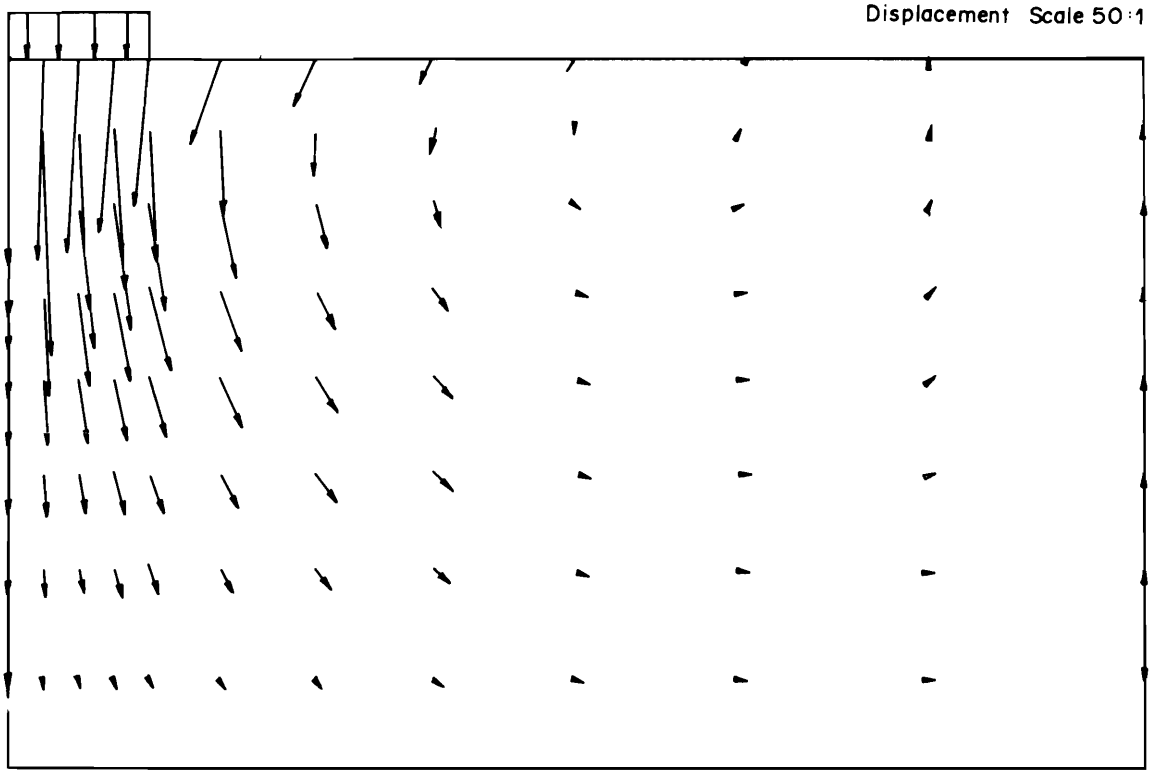

Figure 18. Displacement Vectors Field for the Flexible Footing.

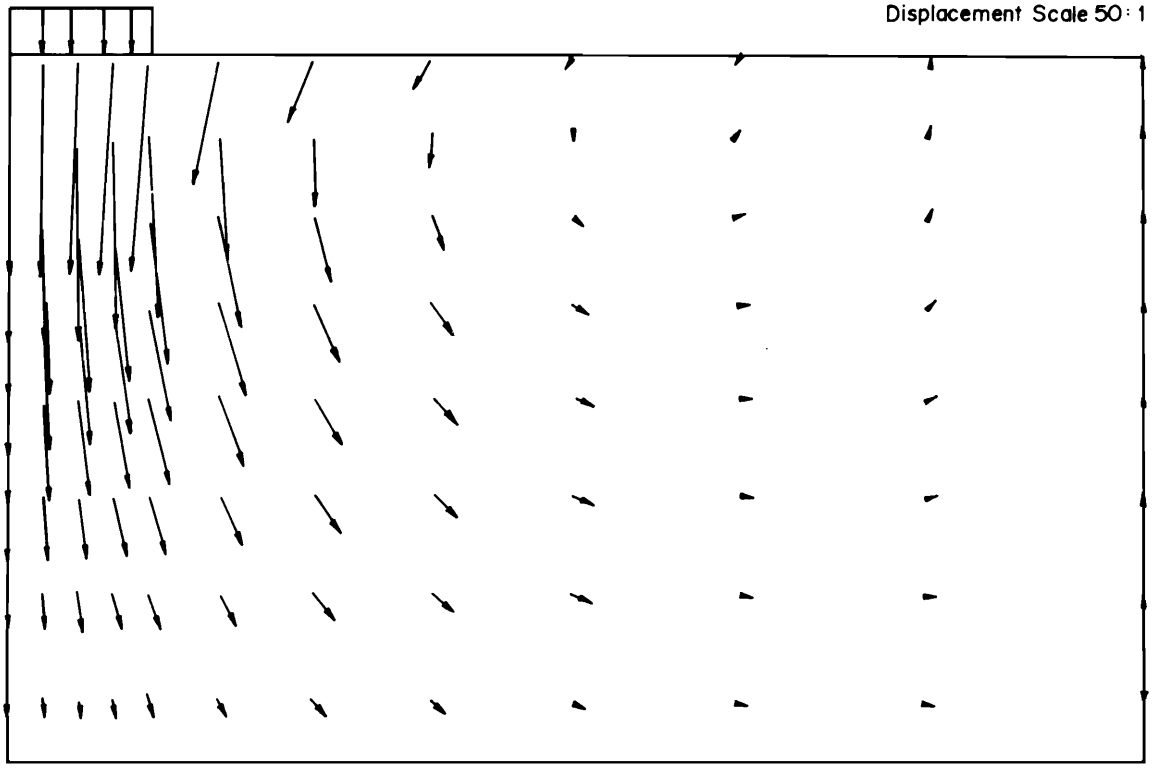

Figure 19. Displacement Vectors Field for the Rigid Footing.

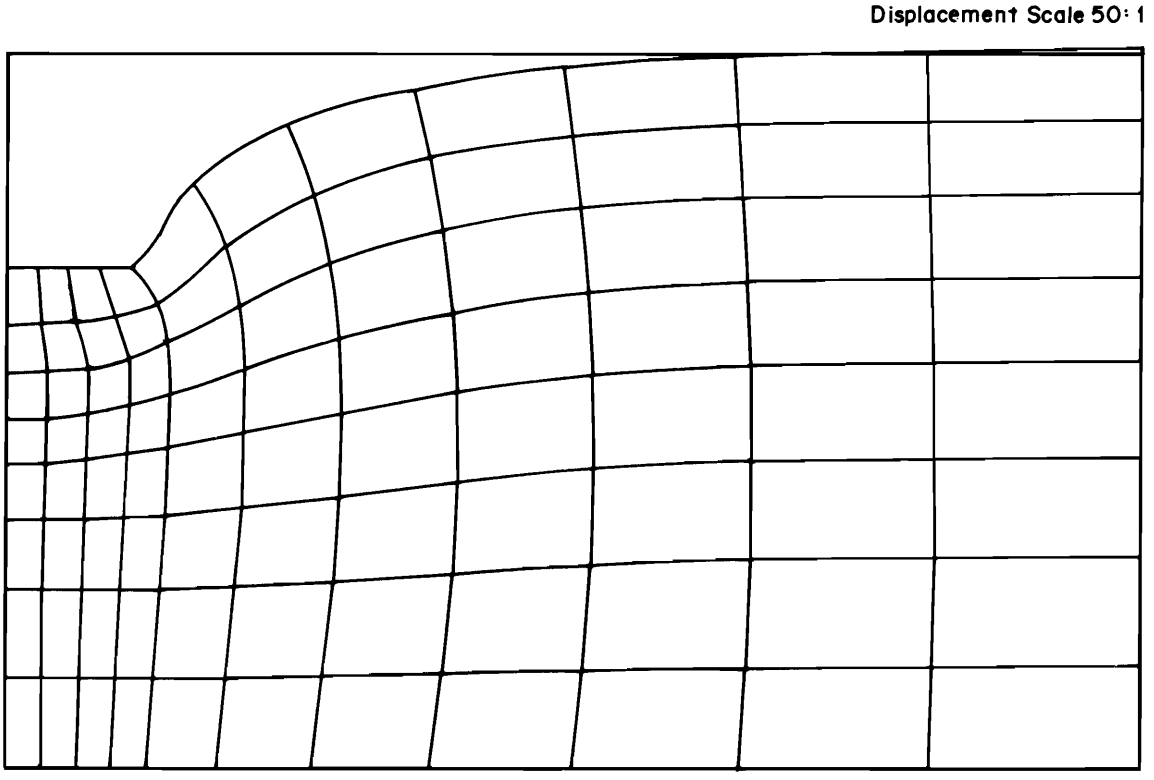

Figure 20. Deformed Mesh for the Flexible Footing.

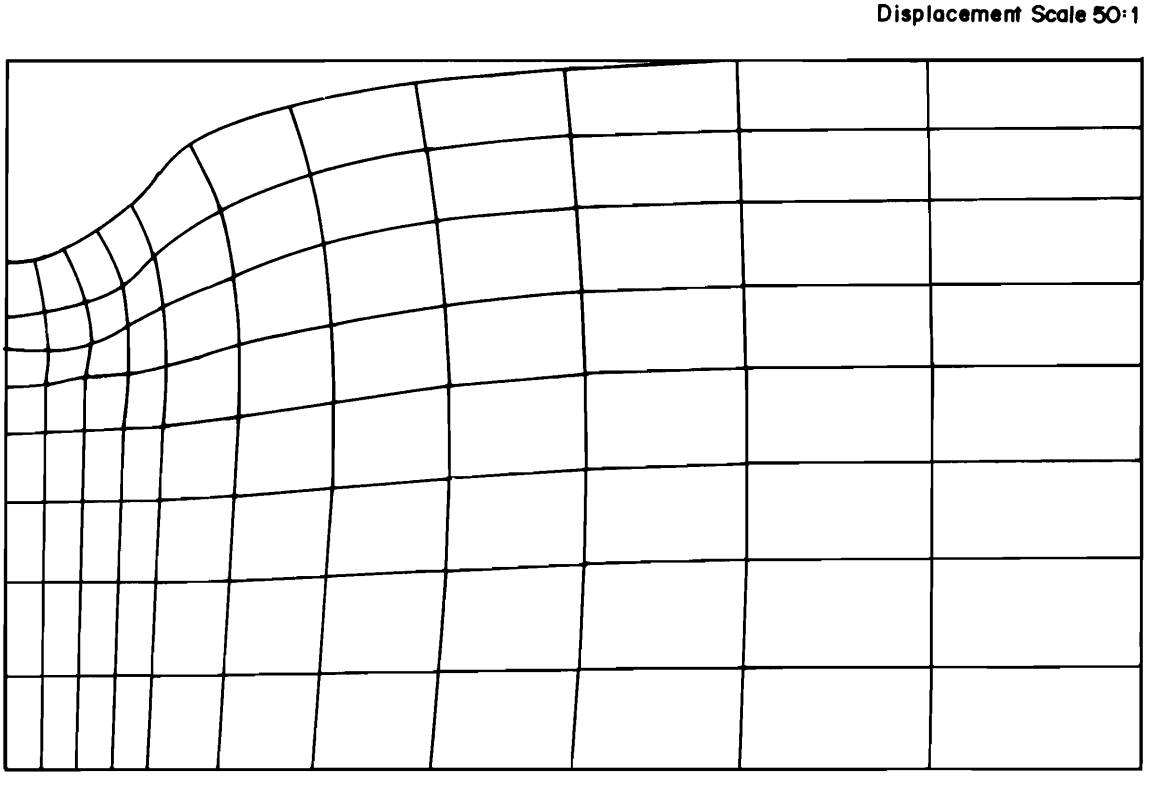

Figure 21. Deformed Mesh for the Rigid Footing.

CONCLUSIONS

The three stress-invariant dependent cap model for cohesionless soil is simple to implement in nonlinear finite element analysis code. It is numerically well-behaved and does not lead to prohibitive computational costs.

Modification of the conventional triaxial testing device to perform tests under different stress paths was done successfully, where tests like triaxial compression, triaxial extension, reduced triaxial compression and reduced triaxial extension can be conducted with it.

The method and techniques adopted for the determination of material constants are efficient and give realistic value.

The results obtained for triaxial specimen loading and the boundary value problems demonstrate that the three stress-invariant dependent cap model describes the stress–strain behavior of Dhahran dune sand quite accurately. The capability of this model to predict variation in strengths along compression and extension paths is found to be excellent.

ACKNOWLEDGEMENTS

The writers wish to record their thanks to Dr. H. N. Al-Ghamdi for his help in the development of the finite element computer program. The authors of this paper would like also to express their appreciation to King Fahd University of Petroleum & Minerals for providing laboratory space and computer facilities required for this research.

APPENDIX. REFERENCES

[1] F. L. DiMaggio and I. S. Sandler, "Material Model for Granular Soils", *J. Eng. Mech. Div., ASCE*, **97(3)** (1971), p. 935.

[2] P. V. Lade and J. M. Duncan, "Elasto-plastic Stress Strain Theory for Cohesionless Soil", *J. Geotech. Eng. Div., ASCE*, **101** (1975), p. 1037.

[3] J. H. Prevost, "Mathematical Modelling of Monotonic and Cyclic Undrained Clay", *Int. J. Num. Analyt. Methods in Geomech.*, **1** (1977), p. 196.

[4] C. S. Desai and M. O. Faruque, "Constitutive Model for (Geological) Materials", *Journal of Eng. Mech. Div., ASCE*, **110(9)** (1984), p. 1391.

[5] H. B. Pooroshasb and S. Pietruszezak, "On Yielding and Flow of Sand; A generalized Two Surface Model", *J. Computer and Geotechnics*, **1** (1985), p. 33.

[6] M. O. Faruque and C. J. Chang, "New Cap Type Model for Failure and Yielding of Pressure Sensitive Materials", *J. Eng. Mech. Div., ASCE*, **112** (1986), p. 1041.

[7] Z. Mroz, V. A. Norris, and O. C. Zienkiewicz, "Application of an Anisotropic Hardening Model in the Analysis of Elastoplastic Deformation of Soils", *Geotechnique*, **29(1)** (1978), p. 1.

[8] M. O. Faruque, "A Third Invariant Dependent Cap Model for Geologic Materials", *Japanese Society of Soil Mechanics and Foundation Engineering*, **27(2)**, 12-20.

[9] J. Podgorski, "General Failure Criterion for Isotropic Media", *J. Eng. Mech. Div., ASCE*, **111** (1985), p. 118.

[10] M. M. Zaman, C. S. Desai, and M. O. Faruque, "An Algorithm for Determining Parameters for Cap Model From Raw Laboratory Test Data", *Proc. 4th Int. Conf. Numer. Methods in Geomech.*, Edmonton, Canada, 1982.

[11] C. S. Desai and H. J. Siriwardane, "Constitutive Laws for Engineering Materials", New Jersey: Prentice-Hall, 1984.

[12] M. O. Faruque, "Development of a Generalized Constitutive Model and its Implementation in Soil-Structure Interaction", *Ph.D. Thesis, University of Arizona, Tucson, Arizona*, 1983.

[13] M. O. Faruque and S. N. Abduljauwad, "Assessment of a Three Stress Invariant Dependent Cap Model for Dhahran Dune Sand", *Proc. First International Conference on Constitutive Laws for Engineering Materials*, Chongqing, China, 1989.

[14] M. O. Faruque and C. S. Desai, "Implementation of a General Constitutive Model for Geological Materials", *International Journal for Numerical and Analytical Methods in Geomechanics*, **9** (1985), p. 415.

[15] M. Azeemuddin, "Constitutive Modelling of Dhahran Dune Sand Using Cap Model", *M.S. Thesis, King Fahd University of Petroleum and Minerals, Dhahran*, 1988.